Local and non-local electron dynamics of Au/Fe/MgO(001) heterostructures analyzed by time-resolved two-photon photoemission spectroscopy

Y. Beyazit,[1] J. Beckord,[1,*] P. Zhou,[1] J. P. Meyburg,[2] D. Diesing,[2] M. Ligges,[1,†] and U. Bovensiepen[1,‡]

[1] *Faculty of Physics and Center for Nanointegration (CENIDE), University of Duisburg-Essen, Lotharstr. 1, 47057 Duisburg, Germany*

[2] *Faculty of Chemistry, University of Duisburg-Essen, Universitätsstr. 5, 45711 Essen, Germany*

(Dated: November 1, 2019)

Employing femtosecond laser pulses in front and back side pumping of Au/Fe/MgO(001) combined with detection in two-photon photoelectron emission spectroscopy we analyze local relaxation dynamics of excited electrons in buried Fe, injection into Au across the Fe-Au interface, and electron transport across the Au layer at 0.6 to 2.0 eV above the Fermi energy. By analysis as a function of Au film thickness we obtain the electron lifetimes of bulk Au and Fe and distinguish the relaxation in the heterostructure's constituents. We conclude further that electron injection across the epitaxial interface proceeds by electron wavepacket propagation. We also show that the excited electrons propagate through Au in a superdiffusive regime determined by few e-e scattering events.

Excited charge carriers relax in metals and semiconductors on femto- to picosecond timescales due to the large phase space for electron-electron (e-e) and electron-phonon scattering [1, 2]. Microscopic insight into these processes was developed by combined efforts of static spectroscopy, spectroscopy in the time domain, and *ab initio* theory [3]. Early optical experiments used back side pump / front side probe schemes and analyzed the propagation dynamics through the bulk of thin films [4]. Time- and angle-resolved two-photon photoelectron spectroscopy exploited the sensitivity to electron energy and momentum and was key to develop a comprehensive understanding of the microscopic nature of the engaged elementary processes which hot electrons experience [5–9]. In heterostrutures such an analysis is challenging but highly desired given the widespread application of these materials. The reason is that photoelectrons are usually sensitive to the surface and the surface near region. In principle this limitation can be overcome using hard X-ray photons in photoemission [10, 11]. Also low kinetic energy of photoelectrons are reported to probe the bulk [12] or buried interface electronic structure [13, 14] in selected cases.

Hot electrons are characterized by their energy above the Fermi energy $E - E_\mathrm{F} \gg k_\mathrm{B}T$, T is the equilibrium temperature, and their momentum $\mathbf{k}$. For a component $k_\perp$ directed from the surface into bulk, transport effects occur. So far, local dynamics at the surface and non-local contributions due to, e.g., transport were distinguished indirectly by analyzing relaxation at surfaces [15–19]. Particular systems allowed a microscopic description of electron propagation through a molecular layer [20] and resonant tunneling across a dielectric film [13].

Electronic transport properties are essential in condensed matter physics. Besides the well-established charge carrier transport in Bloch bands at E_F problems like incoherent hopping in molecular wires [21] and two dimensional materials [22, 23], superdiffusive spin currents [24], and attosecond phenomena at surfaces [25] are important. Recently, the relevance of spin-dependent charge carrier transport in femtosecond magnetization dynamics has spurred the use of back side pumping in optical pump-probe experiments [26–28], which provide energy and momentum integrated information. Back side pump / front side probe studies using photoelectron spectroscopy is highly desired, since it can provide energy and momentum dependent information.

In this letter we report such a back side pump / front side probe photoemission experiment at MgO(001)/Fe/Au as a model system. While for thin Fe and Au films the relaxation agrees for front and back side pump configurations, we identify electron transport for thicker Au films upon back side pumping. By analyzing the dependence of the observed relaxation times on Au film thickness d_Au we distinguish the dynamics in the Au and Fe constituents of the heterostructure.

Fig. 1, top, depicts the experimental configuration. Tunable femtosecond laser pulses are generated by a commercial regenerative Ti:sapphire amplifier (Coherent RegA 9040) combined with a non-collinear optical parametric amplifier (NOPA, Clark-MXR) operating at 250 kHz repetition rate. Here, we use pairs of 2 and 4 eV pulses each of 50 fs pulse duration as pump and probe pulses, respectively. Pump pulses are sent to the Au/Fe/MgO(001) sample kept at room temperature with $\pm 45°$ angle of incidence, see Fig. 1, and reach at first the Au surface in case of front side pumping or are transmitted through MgO(001) and excite electrons of Fe in back side pumping. The incident pump fluence was 50 μJ/cm^2. Probe pulses are in both configurations sent to the Au surface close to 45°. Photoelectrons generated by the probe pulse in two-photon photoemission (2PPE) are analyzed by a self-built electron time-of-flight analyzer [29] and collected in a solid angle within $\pm 11°$ of the surface normal. Au/Fe/MgO(001) heterostructures are

* Current address: University of Zurich, 8057 Zurich, Switzerland
† Current address: Fraunhofer IMS, 47057 Duisburg, Germany
‡ uwe.bovensiepen@uni-due.de

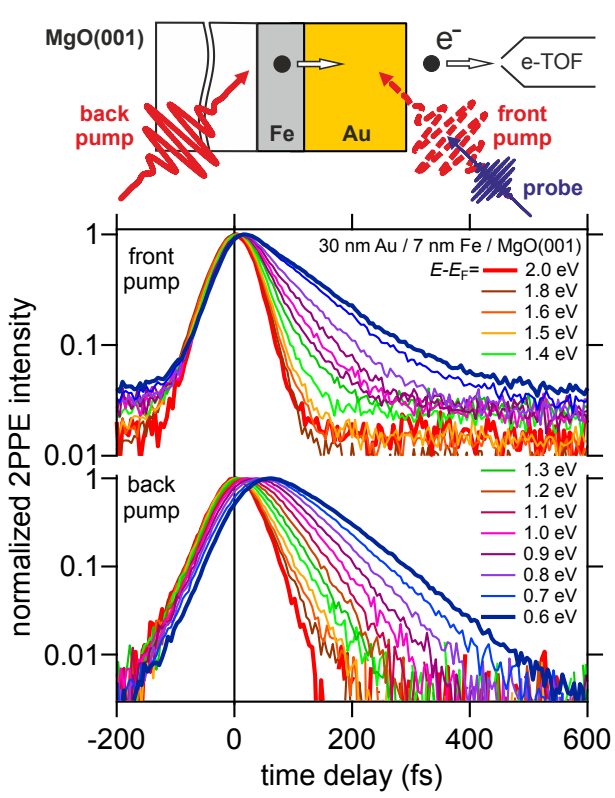

FIG. 1. The top scheme represents the experimental configuration. Either front or back side pumping is applied in combination with the photoemission probing and detection in an electron time-of-flight spectrometer (e-TOF). The 2PPE intensity as a function of pump-probe time delay is shown on a logarithmic scale and normalized to the maximum value. It is plotted for front (top) and back side pumping (bottom) at different energies above the Fermi level $E - E_F$ as indicated.

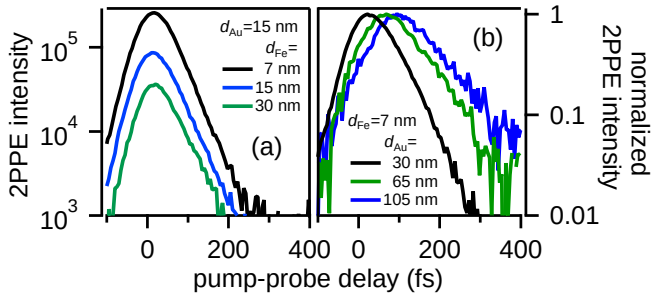

FIG. 2. Time-dependent 2PPE intensity upon back side pumping at $E - E_F$ =1.0 eV shown in (a) for different d_{Fe} and constant d_{Au} and vice versa in (b). In the latter case the 2PPE intensity is normalized to the intensity maximum.

grown by molecular beam epitaxy and are transferred between growth and photoemission chambers under ambient conditions without further cleaning. The layer thickness was determined on a twin sample by profilometer and AFM studies; see also [28, 30].

Fig. 1 shows the time-dependent 2PPE intensity for back and front side pumping at selected energies $E - E_F$ for 30 nm Au/7 nm Fe/MgO(001). Time zero is defined by the fastest signal given by the intensity maximum of electrons at the maximum kinetic energy, given in Fig. 1 by data for $E - E_F = 2.0$ eV. In case of ballistic electron propagation through Au the back side optical excitation would occur at negative time delays determined by the Fermi velocity, which is for Au $v_F \approx 1.4$ nm/fs [4, 31]. The upper graph depicts conventional, front side pump 2PPE data. The lower panel shows results for back side pumping. We emphasize three aspects. (i) The dynamic range obtained with back side pumping is one order of magnitude larger than for front pumping. Since the MgO-Fe and Fe-Au interfaces are well defined we suspect that the static background for front side pump originates from light or electron scattering at the Au-vacuum interface. (ii) The back side pump data exhibit a shift in time delay of the intensity built-up and maximum, which increases with decreasing $E - E_F$. This effect is assigned to delayed arrival of excited electrons at the Au-vacuum interface. (iii) Both data sets exhibit slower intensity relaxation for lower $E - E_F$ due to the respective increase in hot electron lifetime [2].

Fig. 2 compares back side pump 2PPE for different Fe thickness d_{Fe} (a) and for different d_{Au} (b). While in case of increasing d_{Au} transport effects are identified through a time shift in arrival at the Au surface, variation of d_{Fe} results essentially in a loss of intensity. Note that such loss of intensity is also observed with increasing d_{Au}, see supplementary material [32], since only electrons which reach the Au-vacuum interface are detected. These observations support the following concept. The Fe layer acts as the optically excited electron emitter and the Au layer serves as the acceptor hosting electron propagation as depicted by the scheme in Fig. 1.

Time-dependent 2PPE intensities are fitted by a single exponential decay $\propto \exp\frac{t-t_0}{\tau}$ convolved with the cross correlation (XC) of the laser pulses as determined at maximum kinetic energy. Examples of such fits are plotted as insets in Fig. 3(a,b). This fitting determines energy dependent relaxation times $\tau(E)$ and time offsets $t_0(E)$, at which the relaxation starts. Fig. 3 shows $\tau(E)$ and $t_0(E)$ obtained for d_{Au}=30 nm (a) and 5 nm (b) at d_{Fe}=7 nm. We find a decrease in τ with increasing energy and – if compared at identical energies – τ is larger for the thicker than for the thinner Au layer. Front and back side pumping lead to small differences in $\tau(E)$ near 1.2 eV for d_{Au}=30 nm. Such differences were not obtained for d_{Au}=5 nm, neither in τ nor in t_0. For sufficiently thin films transport effects become negligible [17] and d_{Au}=5 nm provides a reasonable reference value in this regard. For d_{Au}=30 nm we identify for back side pumping variations in $t_0(E)$ up to 60 fs while $t_0(E)$ does not vary for front side pumping. The observed increase of t_0 with decreasing $E - E_F$ for back side pumping showcases transport of electrons which are excited in Fe, in-

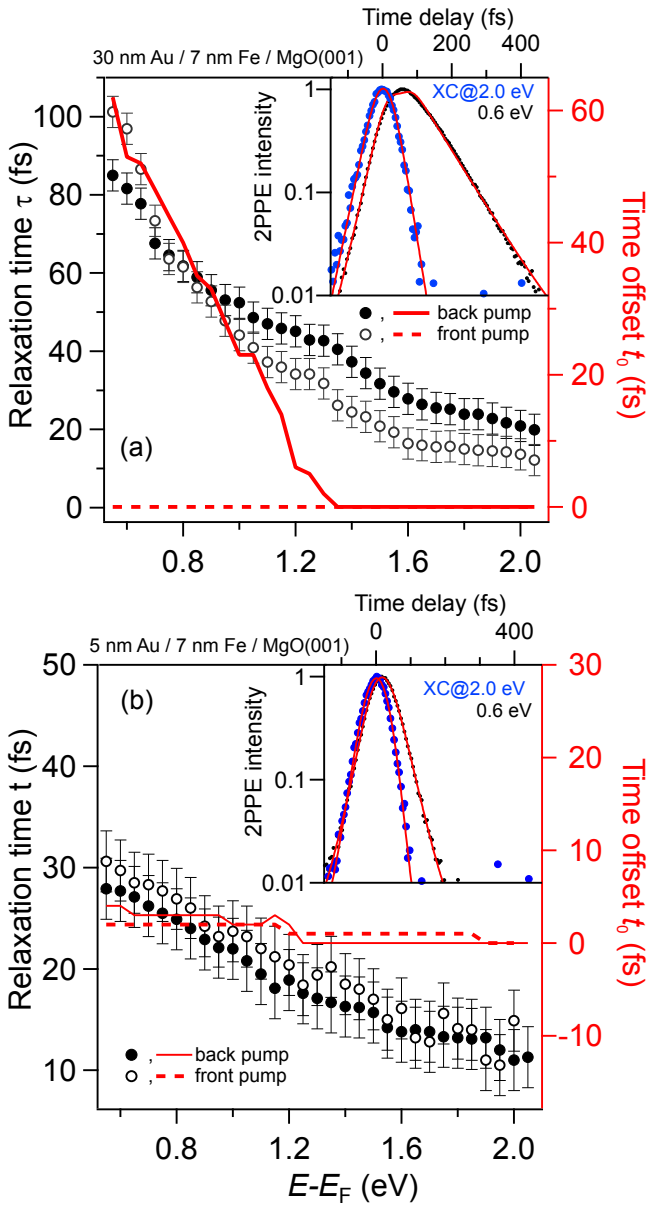

FIG. 3. Left axis: relaxation times τ of hot electrons at energies $E - E_F$ for 30 nm (a) and 5 nm (b) thick Au films on 7 nm Fe on a MgO(001) substrate. Right axis: Time offset t_0, see text. Both quantities are determined by fitting and are given for front and back pumping as indicated. Error bars for t_0 are ±6 fs at 0.7 eV and decrease to ±3 fs at 2.0 eV.

jected into Au across the Fe-Au interface, and propagate through Au towards the Au-vacuum interface, where they are probed in 2PPE. Following bulk optical constants [33] 95% of the absorbed pump pulse intensity excites the 7 nm Fe layer and the 2PPE signal detected at 30 nm Au / 7 nm Fe / MgO(001) is dominated by electrons propagating through Au. This assignment is supported by the increase in t_0 and τ for the larger d_{Au} compared to the thinner one, see Fig. 3. Since relaxation times of hot

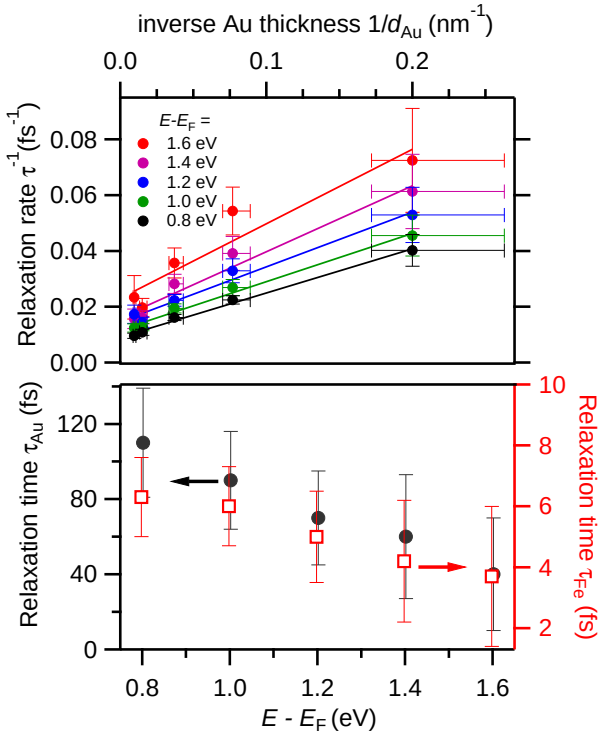

FIG. 4. Top panel: Inverse relaxation times as a function of inverse Au film thickness for different electron energies above E_F. Lines represent linear fits, which determine the relaxation rate in Au as the intercept with the ordinate and in Fe as the slope. Bottom panel: The determined relaxation times τ as determined in the top panel as a function of $E - E_F$ and assigned to hot electron lifetimes in Au and Fe, respectively.

electrons in metals at few eV energy above E_F are determined by inelastic e-e scattering [2], the similar trend of increasing t_0 and τ with decreasing energy indicates that t_0 is determined by inelastic e-e scattering as well. On this basis the electron transport through Au is concluded to be superdiffusive [34]. Reaching the limit of diffusion would require many scattering processes, which is unlikely due to the observation $t_0(E_0) < \tau(E_0)$. Ballistic propagation, on the other hand, would occur for absent relaxation, which disagrees with the observed temporal broadening in time-dependent 2PPE intensities while the electrons propagate through Au, see Fig. 2(b). Given the weak variation of the electron group velocity with respect to the Fermi velocity in Au [31] ballistic propagation is also incompatible with the increase in t_0 observed with decreasing energy. Therefore, a determination of the electron's propagation velocity $v = d_{\mathrm{Au}}/t_0$, which results for d_{Au}=30 nm at $E - E_F$=1.0 eV in v=1.3 nm/fs – a value close to v_F in Au – has to be treated with care. We note that we cannot exclude ballistic propagation of electrons $E - E_F \geq$1.3 eV where we find $t_0 = 0$ fs, which is set by the time zero determination.

We investigated different d_{Au} and identified a thickness dependent $\tau = \tau(d_{\mathrm{Au}})$. The measured values are

smaller than reported for bulk Au [2]. We explain this thickness dependence by two independent relaxation processes which add their rates following Matthiesen's rule

$$\tau^{-1}(d_{\mathrm{Au}}) = \tau_{\mathrm{Au}}^{-1} + \tau_{\mathrm{Fe}}^{-1} = A + \frac{B}{d_{\mathrm{Au}}}. \qquad (1)$$

One process is inelastic e-e scattering in bulk Au. For large d_{Au} the second term in Eq. 1 vanishes and $\tau_{\mathrm{Au}}^{-1} = A$. Assignment of the second process is less obvious. We consider two contributions to the rate $\tau_{\mathrm{Fe}}^{-1} = B/d_{\mathrm{Au}}$: inelastic scattering (i) in the Fe film and (ii) at the Au-Fe interface. By analysis of the dependence on $1/d_{\mathrm{Au}}$, as depicted in Fig. 4 (top), we determine τ_{Au} and τ_{Fe}. The ordinate intercept A increases for larger $E - E_{\mathrm{F}}$ and determines $\tau_{\mathrm{Au}}(E)$. The slope B determines τ_{Fe} which increases also with energy. Fig. 4 (bottom) depicts the obtained relaxation times as a function of energy. Comparison with literature [2] shows that the values obtained for $\tau_{\mathrm{Au}}(E)$ and for $\tau_{\mathrm{Fe}}(E)$ agree with data for bulk Au and Fe, respectively.

The fact that we observe τ_{Au} in back side pump 2PPE in agreement with literature values obtained in front side pump 2PPE is straightforward to understand. A hot electron injected into Au at the Fe-Au interface propagates through the Au film and reaches the surface where it is photoemitted. During the propagation it experiences inelastic e-e scattering with rates of bulk Au and transfers energy to a secondary electron which populates states in the vicinity of E_{F}. We did not take secondary electrons into account in our analysis because we restricted the investigated energy scale to rather high values $E - E_{\mathrm{F}}$, where primary electrons dominate [17]. Secondary electrons start to contribute at half the primary excitation energy [2], which is $E - E_{\mathrm{F}} < 1$ eV for the highest energy electrons at 2 eV studied here.

Access to a buried interface or buried Fe emitter was so far limited in 2PPE due to its sensitivity to the surface or the surface near region. We consider two contributions to the rate B/d_{Au}, see Eq. 1. (i) Inelastic e-e scattering in Fe before electron injection into Au leading to a loss of injection efficiency and (ii) Umklapp scattering of electrons in Au which are injected into Fe across the Au-Fe interface subsequent to electron injection from Fe into Au. Such Umklapp scattering in e-e scattering has been shown for alkali metals to contribute only few percent to the total scattering probability and scattering with phonons enhances this contribution [35]. Since the relaxation of electrons at 0.6 – 2.0 eV investigated here is determined by e-e scattering [2] we discard the phonon enhancement and Umklapp scattering as the leading contribution to τ_{Fe}. We rather consider e-e scattering in the Fe layer to determine τ_{Fe} by a reduced electron injection probability. This assignment is supported by Fig. 2 which reports that increasing d_{Fe} reduces the detected 2PPE signal for back side pumping. The optically excited electrons in Fe redistribute their energy by e-e scattering such that the maximum electron energy is reduced, which lowers the injection probability at the electron energies analyzed on the Au surface. This assignment implies that injection of electrons from Fe into Au proceeds without additional interface scattering in a limit of wavepacket propagation as considered in [26, 30].

In conclusion, we demonstrated a time-domain analysis of electron dynamics in epitaxial MgO(001)/Fe/Au heterostructures with a total thickness of 10 - 100 nm. We distinguish the energy-dependent scattering rates in Fe and Au using optical pumping of Fe and detection at the Au surface by two-photon photoemission. We also identify the electron propagation to proceed in a superdiffusive regime. This separation of electron dynamics in the individual heterostructure constituents showcases the impact our approach might have on future work. A spectroscopy which accesses buried interfaces / media and provides energy-dependent information on electron dynamics is rarely available but provides highly desired insights in heterostructures in general. We expect that this approach will bridge conventional transport measurements and time domain spectroscopy and will facilitate a more comprehensive understanding of electrons dynamics in complex materials. We expect further that this approach to electron transport dynamics will be applied to semiconducting or insulating material systems due to its sensitivity to excited electronic states.

ACKNOWLEDGMENTS

We acknowledge A. Eschenlohr for fruitful discussion. This work was funded by the Deutsche Forschungsgemeinschaft (DFG, German Research Foundation) Projektnummer 278162697 - SFB 1242.

[1] J. Shah, *Ultrafast spectroscopy of Semiconductors and Semiconductor Nanostructures* (Springer, Berlin, Heidelberg, 1999), 2nd ed.
[2] M. Bauer, A. Marienfeld, and M. Aeschlimann, Prog. Surf. Sci. **90**, 319 (2015).
[3] P. M. Echenique, R. Berndt, E. Chulkov, T. Fauster, A. Goldmann, and U. Höfer, Surf. Sci. Rep. **52**, 219 (2004).
[4] S. D. Brorson, J. G. Fujimoto, and E. P. Ippen, Phys. Rev. Lett. **59**, 1962 (1987).
[5] N.-H. Ge, C. M. Wong, R. L. Lingle, J. D. McNeill, K. J. Gaffney, and C. B. Harris, Science **279**, 202 (1998).
[6] M. Weinelt, M. Kutschera, T. Fauster, and M. Rohlfing, Phys. Rev. Lett. **92**, 126801 (2004).
[7] J. Güdde, M. Rohleder, T. Meier, S. W. Koch, and U. Höfer, Science **318**, 1287 (2007).

[8] U. Bovensiepen, H. Petek, and M. Wolf, eds., *Dynamics at Solid State Surfaces and Interfacess*, vol. 1 (Wiley-VCH, Berlin, 2012).

[9] X. Cui, C. Wang, A. Argondizzo, S. Garrett-Roe, B. Gumhalter, and H. Petek, Nature Phys. **10**, 505 (2014).

[10] J. C. Woicik, *Hard X-ray PhotoelectronSpectroscopy* (Springer, Heidelberg, 2016).

[11] L.-P. Oloff, M. Oura, K. Rossnagel, A. Chainani, M. Matsunami, R. Eguchi, T. Kiss, Y. Nakatani, T. Yamaguchi, J. Miyawaki, et al., New J. Phys. **16**, 123045 (2014).

[12] T. Kiss, F. Kanetaka, T. Yokoya, T. Shimojima, K. Kanai, S. Shin, Y. Onuki, T. Togashi, C. Zhang, C. T. Chen, et al., Phys. Rev. Lett. **94**, 057001 (2005).

[13] M. Rohleder, W. Berthold, J. Güdde, and U. Höfer, Phys. Rev. Lett. **94**, 017401 (2005).

[14] L. Rettig, P. S. Kirchmann, and U. Bovensiepen, New J. Phys. **14**, 023047 (2012).

[15] M. Aeschlimann, M. Bauer, S. Pawlik, R. Knorren, G. Bouzerar, and K. H. Bennemann, Appl. Phys. A **71**, 485 (2000).

[16] M. Lisowski, P. A. Loukakos, U. Bovensiepen, J. Stähler, C. Gahl, and M. Wolf, Appl. Phys. A **78**, 165 (2004).

[17] M. Lisowski, P. A. Loukakos, U. Bovensiepen, and M. Wolf, Appl. Phys. A **79**, 739 (2004).

[18] J. P. Gauyacq, A. G. Borisov, and M. Bauer, Prog. Surf. Sci. **82**, 244 (2007).

[19] P. S. Kirchmann, L. Rettig, X. Zubizarreta, V. M. Silkin, E. V. Chulkov, and U. Bovensiepen, Nature Phys. **6**, 782 (2010).

[20] J. Stähler, M. Meyer, D. O. Kusmierek, U. Bovensiepen, and M. Wolf, J. Am. Chem. Soc. **130**, 8797 (2008).

[21] A. A. Kocherzhenko, S. Patwardhan, F. C. Grozema, H. L. Anderson, and L. D. A. Siebbeles, J. Am. Chem. Soc. **131**, 5522 (2009).

[22] A. S. Ngankeu, S. K. Mahatha, K. Guilloy, M. Bianchi, C. E. Sanders, K. Hanff, K. Rossnagel, J. A. Miwa, C. Breth Nielsen, M. Bremholm, et al., Phys. Rev. B **96**, 195147 (2017).

[23] S.-H. Lee, J. S. Goh, and D. Cho, Phys. Rev. Lett. **122**, 106404 (2019).

[24] M. Battiato, K. Carva, and P. M. Oppeneer, Phys. Rev. Lett. **105**, 27203 (2010).

[25] Z. Tao, C. Chen, T. Szilvási, M. Keller, M. Mavrikakis, H. Kapteyn, and M. Murnane, Science **353**, 62 (2016).

[26] A. Melnikov, I. Razdolski, T. O. Wehling, E. T. Papaioannou, V. Roddatis, P. Fumagalli, O. Aktsipetrov, A. I. Lichtenstein, and U. Bovensiepen, Phys. Rev. Lett. **107**, 76601 (2011).

[27] N. Bergeard, M. Hehn, S. Mangin, G. Lengaigne, F. Montaigne, M. L. M. Lalieu, B. Koopmans, and G. Malinowski, Phys. Rev. Lett. **117**, 147203 (2016).

[28] I. Razdolski, A. Alekhin, N. Ilin, J. P. Meyburg, V. Roddatis, D. Diesing, U. Bovensiepen, and A. Melnikov, Nature Commun. **8**, 15007 (2017).

[29] P. S. Kirchmann, L. Rettig, D. Nandi, U. Lipowski, M. Wolf, and U. Bovensiepen, Appl. Phys. A **91**, 211 (2008).

[30] A. Alekhin, I. Razdolski, N. Ilin, J. P. Meyburg, D. Diesing, V. Roddatis, I. Rungger, M. Stamenova, S. Sanvito, U. Bovensiepen, et al., Phys. Rev. Lett. **119**, 17202 (2017).

[31] D. M. Nenno, B. Rethfeld, and H. C. Schneider, Phys. Rev. B **98**, 224416 (2018).

[32] See Supplemental Material.

[33] J. H. Weaver, C. Krafka, D. W. Lynch, and E. E. Koch, *Optical Properties of Metals* (Fachinformationszentrum, Karlsruhe, 1981), vol. 18-1, 18-2 of *Physics Data*.

[34] M. Battiato, K. Carva, and P. M. Oppeneer, Phys. Rev. B **86**, 024404 (2012).

[35] A. H. MacDonald, R. Taylor, and D. J. W. Geldart, Phys. Rev. B **23**, 2718 (1981).